Open access • Journal Article • DOI:10.1029/98JD02593

Effects of black carbon content, particle size, and mixing on light absorption by aerosols from biomass burning in Brazil — Source link

J. Vanderlei Martins, Paulo Artaxo, Catherine Liousse, Jeffrey S. Reid ...+2 more authors

Published on: 27 Dec 1998 - Journal of Geophysical Research (John Wiley & Sons, Ltd)

Topics: Carbon black, Absorption (electromagnetic radiation), Nephelometer, Particle size and Soot

Effects of black carbon content, particle size, and mixing on light absorption by aerosols from biomass burning in Brazil

J. Vanderlei Martins, Paulo Artaxo, Catherine Liousse, Jeffrey Reid, Peter Hobbs, Yoram Kaufman

JOURNAL OF GEOPHYSICAL RESEARCH, VOL. 103, NO. D4, PAGES 32,041–32,050, DECEMBER 27, 1998

Effects of black carbon content, particle size, and mixing on light absorption by aerosols from biomass burning in Brazil

J. Vanderlei Martins,[1,2,3] Paulo Artaxo,[1] Catherine Liousse,[4] Jeffrey S. Reid,[2] Peter V. Hobbs,[2] and Yoram J. Kaufman[3]

Abstract. Black carbon mass absorption efficiencies of smoke particles were measured for various types of biomass fires during the Smoke, Clouds, and Radiation–Brazil (SCAR-B) experiment using thermal evolution measurements for black carbon and optical absorption methods. The obtained results range between 5.2 and 19.3 $m^2\ g^{-1}$ with an average value of 12.1 ± 4.0 $m^2\ g^{-1}$. Particle size distributions and optical properties were also measured to provide a full set of physical parameters for modeling calculations. Mie theory was used to model the optical properties of the particles assuming both internal and external mixtures coupling the modeling calculations with the experimental results obtained during the campaign. For internal mixing, a particle model with a layered structure consisting of an absorbing black carbon core, surrounded by a nonabsorbing shell, was assumed. Also, for internal mixing, a discrete dipole approximation code was used to simulate packed soot clusters commonly found in electron microscopy photographs of filters collected during the experiment. The modeled results for layered spheres and packed clusters explain black carbon mass absorption coefficients up to values of about 25 $m^2\ g^{-1}$, but measurements show even higher values which were correlated with the chemical composition and characteristics of the structure of the particles. Unrealistic high values of black carbon absorption efficiencies were linked to high concentrations of K, which influence the volatilization of black carbon (BC) at lower temperatures than usual, possibly causing artifacts in the determination of BC by thermal technique. The modeling results are compared with nephelometer and light absorption measurements.

1. Introduction

Light absorption by aerosol particles has a heating effect in the atmosphere, which contrasts with the cooling effect by nonabsorptive particles. The balance between the cooling and the heating effects depends on the absorption and scattering properties of the particles. Smoke particles produced by biomass burning have a significant fraction of light-absorbing material composed by black carbon particles. Black carbon is the only important absorber to be taken into account in radiative transfer calculations of smoke aerosols. The same amount of BC for different types of mixing may result in fairly different absorption properties. The efficiency with which a certain amount of BC will absorb light is expressed by a BC mass absorption efficiency (αa_{BC}). This coefficient relates the amount of BC in the particle with the light absorption cross section and depends on the size of particles and on the type of mixing between BC and nonabsorbing components (such as organic matter and sulfates). In external mixtures consisting of individual pure BC particles in parallel with nonabsorbing particles, the BC mass absorption efficiency is, in general, about the same as for pure BC particles. However, for smoke aerosol, it is likely that BC particles that form at relatively high temperatures will be coated by a nonabsorbing shell (to form an internal mixture). The external shell is likely formed by gas-to-particle conversion and condensation of volatile compounds. Thus a reasonable model for biomass burning particles is a layered sphere, with a highly absorbing BC core surrounded by a nonabsorbing shell.

Ackerman and Toon [1981] explored the optical properties of internal and external mixtures using the layered-sphere model and volume-homogeneous mixtures, where the absorbing material is homogeneously mixed with nonabsorbing compounds. Another type of internal mixture commonly found in smoke aerosols are long-chain aggregates of BC particles formed at high temperatures close to the fire. These chain aggregates can also be coated with nonabsorbing materials to form an internally mixed heterogeneous structure. After aging and interactions with water vapor and clouds, these opened clusters usually collapse to form closely packed spherical-like structures [*Hallet et al.*, 1989]. These packed structures are likely to be externally coated and also have nonabsorbing material in its internal structure. Figure 1 shows examples of some possible internal and external mixtures of BC particles and nonabsorbing materials in smoke from biomass fires.

In the present study, we use Mie theory to estimate the mass absorption efficiency of BC particles internally and externally mixed with nonabsorbing materials. Calculations for particles with a layered structure were performed using a Mie code developed by *Ackerman and Toon* [1981], as further developed and made available by W. Wiscombe. Closely packed BC clus-

[1]Instituto de Física, Universidade de São Paulo, São Paulo, Brazil.
[2]Department of Atmospheric Sciences, University of Washington, Seattle.
[3]NASA Goddard Space Flight Center, Greenbelt, Maryland.
[4]Centre de Faibles Radioactivites, CNRS-CEA, Gif sur Yvette, France.

Paper number 98JD02593.
0148-0227/98/98JD-02593$09.00

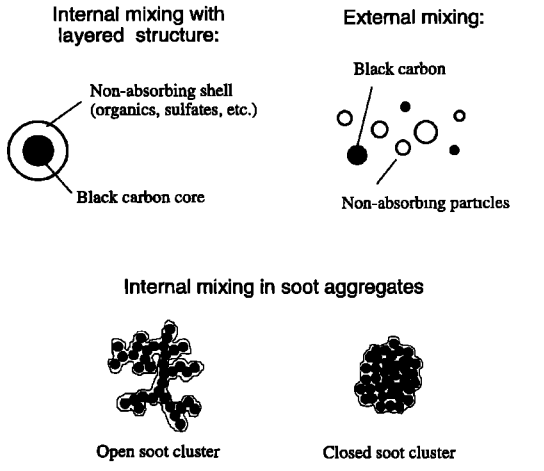

Figure 1. Examples of some possible mixtures between black carbon (BC) and nonabsorbing materials in smoke particles.

ters were simulated by a three-dimensional mathematical structure with thousands of dipoles, the optical properties of which were calculated using the discrete dipole approximation [*Draine and Flatau*, 1994; *Purcell and Pennypacker*, 1973]. Dipole calculations were performed using the code DDSCAT, made available by B. Draine and P. Flatau. Results from closed clusters are compared with those from the layered-sphere model and with the Maxwell-Garnett average field theory for homogeneous internally mixed materials [*Bohren and Huffman*, 1983]. The modeling results are compared with measurements of BC mass absorption efficiency obtained during the SCAR-B field project in Brazil.

2. Theoretical Modeling

The mass absorption efficiency of an aerosol particle (αa) is defined as the absorption coefficient of the particles (m^{-1}) divided by the particle mass concentration (g m^{-3}). Similarly, the BC mass absorption efficiency (αa_{BC}) is defined as the absorption coefficient of the particles (m^{-1}) divided by the mass concentration of black carbon (g m^{-3}) in the aerosol. The BC mass absorption efficiency indicates how efficiently a certain amount of BC absorbs light for different types of particle mixing and sizes. Figure 2 shows Mie calculations of the BC mass absorption efficiency for pure BC spheres (at $\lambda = 0.55$ μm) as a function of the particle radius. The BC mass absorption efficiency for pure BC particles ($\rho = 1.85$ g cm^{-3}) remains below 10 m^2 g^{-1}, regardless of particle size and for three values of the complex refractive index covering the range commonly found in the literature [*Horvath*, 1993a]. Calculations of the BC mass absorption efficiencies over a realistic accumulation mode biomass burning particle size distribution [e.g., *Reid et al.*, this issue (b)] produces values much lower than 10 m^2 g^{-1}. Internally mixed particles composed of an absorbing core surrounded by a nonabsorbing shell have, in general, a greater BC mass absorption efficiency than pure BC particles. This is because the nonabsorbing shell increases the total cross-sectional area of the particle and focuses light toward the absorbing core, causing the same amount of BC in the mixed structure to absorb more than pure BC particles.

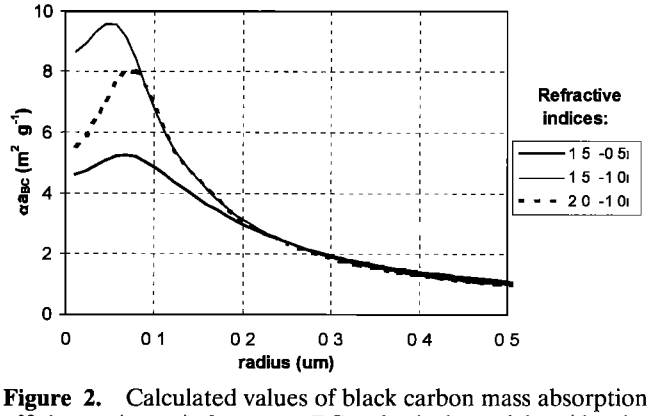

Figure 2. Calculated values of black carbon mass absorption efficiency (αa_{BC}) for pure BC spherical particles (density 1.85 g cm^{-3}) at a wavelength of 0.55 μm. Three complex refractive indices (n), spanning values commonly found in the literature, were used in these calculations ($n = 1.5–0.5i$, $n = 1.5–1.0i$, and $n = 2.0–1.0i$).

Figure 3 shows calculated BC mass absorption efficiency for particles with a BC core surrounded by a nonabsorbing shell. Along the text, shell radius is defined as equal to the particle radius. It can be seen that for particles with a layered structure the value of αa_{BC} depends on the fraction of BC in each particle and on the size of the particles, but it can be much larger than that for pure BC particles. For the studied parameters, the larger the particle radius the larger the effect of the nonabsorbing coating in αa_{BC}, up to a maximum αa_{BC} value for a particle radius of about 0.25 μm. For a BC fraction of 0.5%, and monodispersed particles with an external radius of 0.25 μm, αa_{BC} can reach values as high as 30 m^2 g^{-1}. The different behavior as a function of the shell radius can be explained by the relative size of the BC core, which is determined by the fraction BC/TPM (black carbon divided by total particle mass), the external particle radius, and the density of each component. The shell radius is also important in determining the value of the mass absorption coefficient. For a particle radius about 0.05 μm, the BC mass absorption effi-

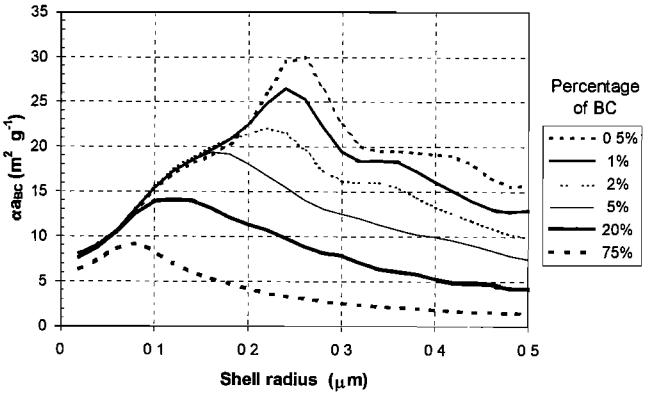

Figure 3. Calculated values of black carbon mass absorption efficiency (αa_{BC}) at $\lambda = 0.55$ μm for an internal mixture of BC and nonabsorbing material in a layered structure. The particle structure consists of an absorbing BC core with a surrounding nonabsorbing shell. The refractive index of the BC was assumed to be $2.0–1.0i$, the density 1.85 g cm^{-3}; for the nonabsorbing shell, the refractive index was assumed to be $1.5–10^{-6}i$ and the density 1.5 g cm^{-3}. The amount of BC and the radius of the shell determine the radius of the BC core. The radius of the shell is defined in this work as equal to the radius of the particle.

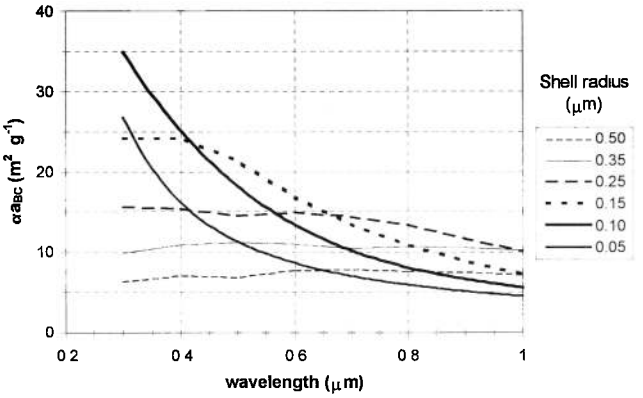

Figure 4. Calculated values of black carbon mass absorption efficiency (αa_{BC}) as a function of the wavelength for several particle radii based on Mie calculations for the layered-sphere model. Particle structure is an absorbing BC core (5% in mass) and a nonabsorbing external shell. Optical parameters are the same as for Figure 3.

ciency is around 10 m^2 g^{-1} and is almost independent of the ratio BC/TPM. Several authors obtained values around 10 m^2 g^{-1} for αa_{BC} of aerosol particles [*Clarke et al.*, 1987; *Japar et al.*, 1986; *Roessler and Faxvog*, 1980]. The value of αa_{BC} is also dependent on the real part of the refractive index of the nonabsorbing shell. For a range of real refractive indices around values reported in the literature for organic materials and sulfate, higher refractive indices will produce higher values of αa_{BC} (at $\lambda = 0.55$ μm).

Spectral measurements of light absorption associated with measurements of the particle size distributions can be useful in determining the type of mixing between BC and nonabsorbing particles. The wavelength dependence of the light absorption depends on the sizes of the absorbing particles. Figure 4 shows an example of the spectral dependence of the BC mass absorption efficiency for several particle sizes based on the layered-sphere model with an absorbing core and a nonabsorbing shell with 5% BC in mass. The results show that smaller particles (0.05 to 0.15 μm) have stronger wavelength dependence for light absorption than larger particles. This suggests that spectral measurements of light absorption by aerosol particles can provide information on the type of mixing and on the size of the absorbers.

Other factors, such as the shape and structure of the particles, can affect the BC mass absorption efficiency. Black carbon is commonly found in large chain aggregates close to the fires. The optical properties of these fresh aggregates have been estimated to be equivalent to individual pure BC particles. These aggregates can also have a nonabsorbing external layer, and after interacting with water vapor and clouds, they can collapse to form more closely packed structures [*Hallet et al.*, 1989]. Scanning electron microscopy (SEM) photographs show that in some cases, most of the particles in regional hazes in Brazil are composed of compact closed clusters, with the particle radius varying over the whole size distribution [*Martins et al.*, this issue]. These closed structures have different optical properties from the initial fresh chain aggregates. Depending on size ranges and structures, the BC mass absorption efficiency for these packed clusters with a nonabsorbing layer will be larger than those of pure BC particles.

Figure 5a shows a transmission electron microscope (TEM) photograph of a smoke particle composed of a closed cluster aggregate and, apparently, a coating of lower density material. Figure 5b illustrates the mathematical model we used to calculate the optical properties of such closed clusters using the discrete dipole approximation code (DDSCAT). Each dot in Figure 5b represents a single dipole, with different symbols for

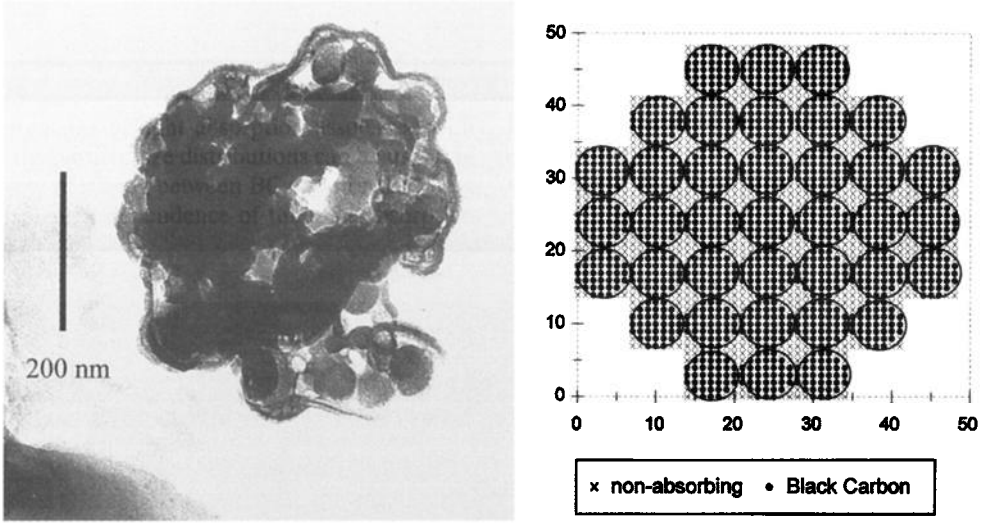

Figure 5. (a) Transmission electron microscopy photograph of a closely packed BC cluster from biomass burning. The structure shows evidences of a particle coating with a different material from that of the isolated spheres. Photograph courtesy of F. Echalar, Institute of Physics, University of São Paulo. (b) Three-dimensional mathematical structure used for simulating internal mixtures of a closely packed cluster using the discrete dipole approximation. Each dot in the figure represents a single dipole; the large circles composed of many dots correspond to single BC particles.

BC and nonabsorbing materials. The black dots represent dipoles with the dielectric properties of BC, the x symbols are dipoles with dielectric properties of nonabsorbing materials. A complex refractive index of $2.0–1.0i$ was assumed for BC and $1.5–1.0 \times 10^{-6}i$ for nonabsorbing particles, with densities of 1.85 and 1.5 g cm^{-3}, respectively. The modeled structure is three dimensional with BC particles in touch with each other and all the free spaces filled with nonabsorbing material. This mixture results in a volume ratio (V_{BC}/V_{tot}) of 0.52, which means that BC corresponds to 64% of the particle mass. It is important to recall that even if the bulk BC/TPM fraction in aerosols are of the order of 5–15%, isolated particles may have a higher BC fraction depending on the particular mixture for each case (e.g., Figure 5a: particle is likely composed predominantly by BC). The BC mass absorption efficiency (αa_{BC}) for this structure was calculated using the DDSCAT code.

Figure 6 compares results from the packed cluster structure with αa_{BC} for pure BC particles and for the layered-sphere model. For all particle radius, αa_{BC} for the closed cluster is larger than for pure BC particles, with a peak of 10 m^2 g^{-1} at a particle radius about 0.1 μm for the given BC/TPM ratio. The closed cluster also showed αa_{BC} values up to 35% higher than results for the layered sphere model for particle radius larger than 0.1 μm. Moreover, also in Figure 6 these results are compared with results from the Maxwell-Garnett mean field theory. In this theory, one determines average dielectric functions for the composed material, which are then used in a Mie code for estimating optical properties. The mixing rule used for this calculation considers a two component mixture with a nonabsorbing matrix containing spherical absorbing inclusions pondered by volume. The Maxwell-Garnet theory and the mixing rule used in this work is described in details by *Bohren and Huffman* [1983]. Despite problems in determining average effective refractive indices for mixed materials, we present an intercomparison of the DDSCAT results and the mean field theory as an example of a simple model for a complex structure. Good agreement was found between the DDSCAT results and the Maxwell-Garnet theory combined with Mie calculations in estimating αa_{BC} over a large range of particle sizes. There was also good agreement for the particle mass scattering coefficient, although this does not assure that the mean field theory will reproduce all the optical properties of closed clusters at any wavelength, mixing ratio, or particle size. By analogy with the layered-sphere model, a smaller mixing ratio will provide a large αa_{BC} value. Extrapolations using the mean field theory suggest that these packed clusters should not reach αa_{BC} values larger than 20 m^2 g^{-1} for realistic particle sizes and mixing ratios. Therefore the obtained results are in the same range as those obtained with the layered-sphere model.

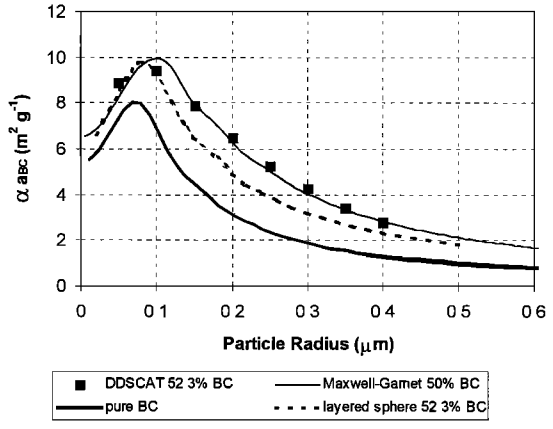

Figure 6. Calculated values of black carbon mass absorption efficiency for a BC cluster (at $\lambda = 0.55$ μm) with a nonabsorbing coating around individual particles versus the particle radius using the discrete dipole approximation (DDSCAT). Results from DDSSCAT are compared with pure BC particles (solid curve), layered-sphere model, and calculations using the Maxwell-Garnett theory considering a volume ratio of about 52 or 64% in mass.

3. Measurements

3.1. Techniques

Black carbon mass absorption efficiencies for aerosol particles were obtained for all samples collected simultaneously in Nuclepore and Quartz filters during the Smoke, Clouds, and Radiation–Brazil (SCAR-B) experiment. The determination of αa_{BC} depends on measurements of the absorption coefficient and BC mass concentration. Measurements of light absorption by aerosols have been discussed by many authors [e.g., *Horvath*, 1993a, b; *Clarke*, 1982a, b; *Clarke et al.*, 1987, 1996; *Campbell et al.*, 1995; *Campbell and Cahill*, 1996; *Hanel et al.*, 1982; *Delumyea et al.*, 1980]. Most of the methods applied on filters produce artifacts that depend on particle loading, type of filter, and type of particles but, on the other hand, have the advantage of concentrating the particles in a small volume for further analysis. The aethalometer technique combines automated optical attenuation measurements in filters with good time resolution depending on mass concentrations [*Hansen et al.*, 1982; *Ruoss et al.*, 1993]. Light absorption techniques require empirical calibrations and intercomparisons with different methods for quality assurance. During SCAR-B, light absorption was measured simultaneously by several techniques (optical extinction cell, integrating plate technique on Teflon filters, optical reflectance on Nuclepore filters, and absorption photometry or aethalometer technique) aboard the University of Washington (UW) C131-A aircraft; *Reid et al.* [this issue (a)] present an intercomparison of these techniques for the SCAR-B data set, considering a combination of the UW extinction cell plus a nephelometer as a reference methodology [*Weiss and Hobbs*, 1992]. *Reid et al.* [this issue (a)] concluded that for the various techniques used on the C-131A, optical reflectance (OR) provided the best correlation ($r = 0.9$) with light absorption measurements from the Weiss-Hobbs optical extinction cell (OEC) over several orders of magnitude. Reflectance techniques have been applied by other authors to obtain optical properties of aerosol particles [*Lindberg and Laude*, 1977; *Patterson and Marshall*, 1982]. *Hanel* [1988] discusses a photometric methodology for measuring light absorption by aerosol particles and concludes that its results are equivalent to a diffuse reflectance technique and to calorimetric measurements [*Hanel and Hillenbrand*, 1989].

Particulate carbon concentrations in the aerosol were determined by thermal analysis [*Cachier et al.*, 1989] of quartz filters at the Centre de Faibles Radioactivites, CNRS-CEA, Gif sur Ivette, France. The exposed filters were subjected to HCl vapors for 24 hours in order to remove carbonates. The carbon remaining on the filters after this treatment is referred to as total atmospheric particulate carbon (TC). Both total and black carbon measurements were performed on filter aliquots

by coulometric titration with a Ströhlein Coulomat®702C. The black carbon fraction (BC_{Th}) is analyzed after the thermal removal of the organic compounds at 340°C during 120 min under pure oxygen. OC is assumed to be the difference between TC and BC. It must be recalled, however, that the BC and OC separation is method dependent [*Reid et al.*, this issue (a); *Petzold and Niessner*, 1995]. The published uncertainty in the BC content is of the order of 10% when BC/TC ratio is in the 10–35% range, which corresponds to 70% of samples for the SCAR-B campaign. It must be noted that following *Reid et al.* [this issue (a)] and for the SCAR-B data set, BC concentrations could be increased by 25%, due to thermal method sensitivity to catalytic reactions with K and Na [*Novakov and Corrigan*, 1995]. The Nuclepore, Quartz, and Teflon filters were collected in parallel in a grab-bag sampling system aboard the UW C131-A aircraft using the same inlet. Therefore because of sampling similarity with the quartz filters and good correlation with the OEC results ($r = 0.9$), absorption measurements from Nuclepore filters were considered in this work to calculate the absorption coefficients.

Several other aerosol properties were measured simultaneously, including particle size distributions, light scattering, and humidification factors [*Hobbs*, 1996; *Reid et al.*, this issue (b); *Reid and Hobbs*, this issue]. Samples were collected in different conditions and environments, including smoke plumes, regional hazes, background air, and clouds. Nuclepore filters were also subjected to PIXE (proton-induced X-ray emission), SEM (scanning electron microscopy), and gravimetric analysis. The Teflon filters were analyzed gravimetrically and by ion chromatography. The elemental and ionic compositions provided information on the dependence of αa_{BC} on the chemical composition of the particle, and the electron microscopy results provided information on the micromorphology and structure of the particles.

3.2. Results

Figure 7 shows a histogram of the measured BC mass absorption efficiencies for all the Nuclepore filters collected in parallel with quartz filters. The distribution of BC mass absorption efficiencies shows αa_{BC} values between 5.2 and 58.2 $m^2\ g^{-1}$ separated in two groups with distinct chemical signatures. The first group has a K/BC_{Th} ratio smaller than 0.78 and αa_{BC} values between 5.2 and 19.3 $m^2\ g^{-1}$, with an average value of 12.1 ± 4.0 $m^2\ g^{-1}$. The second group for K/BC_{Th} larger than 0.78 shows very scattered results for αa_{BC} with values between 18.0 and 58.2 $m^2\ g^{-1}$ and an average value of 37 ± 14 $m^2\ g^{-1}$. This separation is strongly observed in the relationship of αa_{BC} and the concentrations of K, Ca, and Mg for each sample, as it can be seen in Figures 8a–8c. High values of αa_{BC} correlate well with high K, Ca, and Mg concentrations. According to *Novakov and Corrigan* [1995], K has a catalytic effect on BC, lowering its volatilization temperature and causing artifacts on BC measurements obtained by thermal evolution techniques. This effect can explain the separation of αa_{BC} in two different groups and suggests an upper limit value of $K/BC_{Th} = 0.78$, under which BC_{Th} presented reasonable values. The authors also suggest a similar effect associated with Na, but we did not find any association between the ratio Na/BC_{Th} and αa_{BC}. Thus samples with $K/BC_{Th} < 0.78$ were selected for the measurement of αa_{BC} in this data set. This procedure needs to be studied and generalized for other data sets, suggesting a quality assurance protocol for thermal BC data.

The $K/BC_{Th} = 0.78$ upper limit is also in accordance with the optical modeling calculations presented in section 2. As showed in Figure 3, the maximum value for a monodispersed particle size distribution using the layered-sphere model is about 30 $m^2\ g^{-1}$. Integrating over a realistic accumulation-mode size distribution for biomass burning particles [e.g., *Reid et al.*, this issue (b)], this value reaches a maximum of about 25 $m^2\ g^{-1}$. Similar values were found for a packed cluster of BC particles embedded in a nonabsorbing matrix. Also, αa_{BC} values commonly reported in the literature are generally below 25 $m^2\ g^{-1}$ [e.g., *Liousse et al.*, 1993; *Horvath*, 1993a; *Roessler and Faxvog*, 1980]. However, *Chylek et al.* [1995] discuss the possibility of BC mass absorption efficiency reaching values up to 100 $m^2\ g^{-1}$ in special circumstances (e.g., water droplets with a small BC core out of center).

Using the layered-sphere model described in section 2, the optical properties of the aerosol particles were estimated on the basis of the parameters measured on the UW C131-A aircraft, namely, simultaneous measurements of light absorption and mass concentrations (Nuclepore and Teflon filters), BC_{Th} (quartz filters), particle size distribution with a passive cavity aerosol spectrometer probe (PCASP) and a differential mobility particle sizer (DMPS), and total light scattering and backscattering at three wavelengths. The PCASP measures particles with diameter between 0.1 and 3.0 μm, while the DMPS measures particles diameter in the range of 0.01–0.6 μm. Five cases were modeled assuming a constant fraction of BC for all the particles in the size distribution. For the BC core, a complex refractive index of $2.0–1.0i$ at 0.55 μm was assumed, with a density of 1.85 g cm^{-3}. Particle size distributions were considered to be lognormal. Figure 9 shows a comparison between the measured values of αa_{BC} versus the relative amount of thermal BC in each sample separating cases with $K/BC_{Th} < 0.78$. Calculated results using the layered-sphere model with three measured particle size distributions are superimposed on the experimental values, as well as the asymptotic αa_{BC} value for pure BC particles with similar particle size distributions. In this case, the αa_{BC} values for pure BC particles represent external mixing between BC and non-

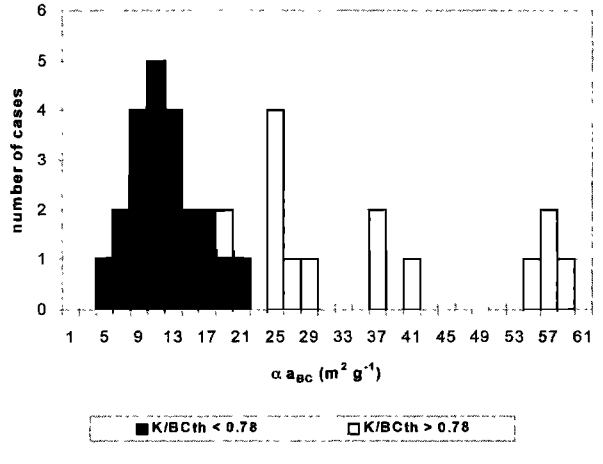

Figure 7. Histogram of measured BC mass absorption efficiencies obtained during SCAR-B. Results are separated in two groups with $K/BC_{Th} < 0.78$ and $K/BC_{Th} > 0.78$. As discussed in the text, estimates of αa_{BC} were obtained based on the group with $K/BC_{Th} < 0.78$ producing an average αa_{BC} = 12.1 ± 4.0 $m^2\ g^{-1}$.

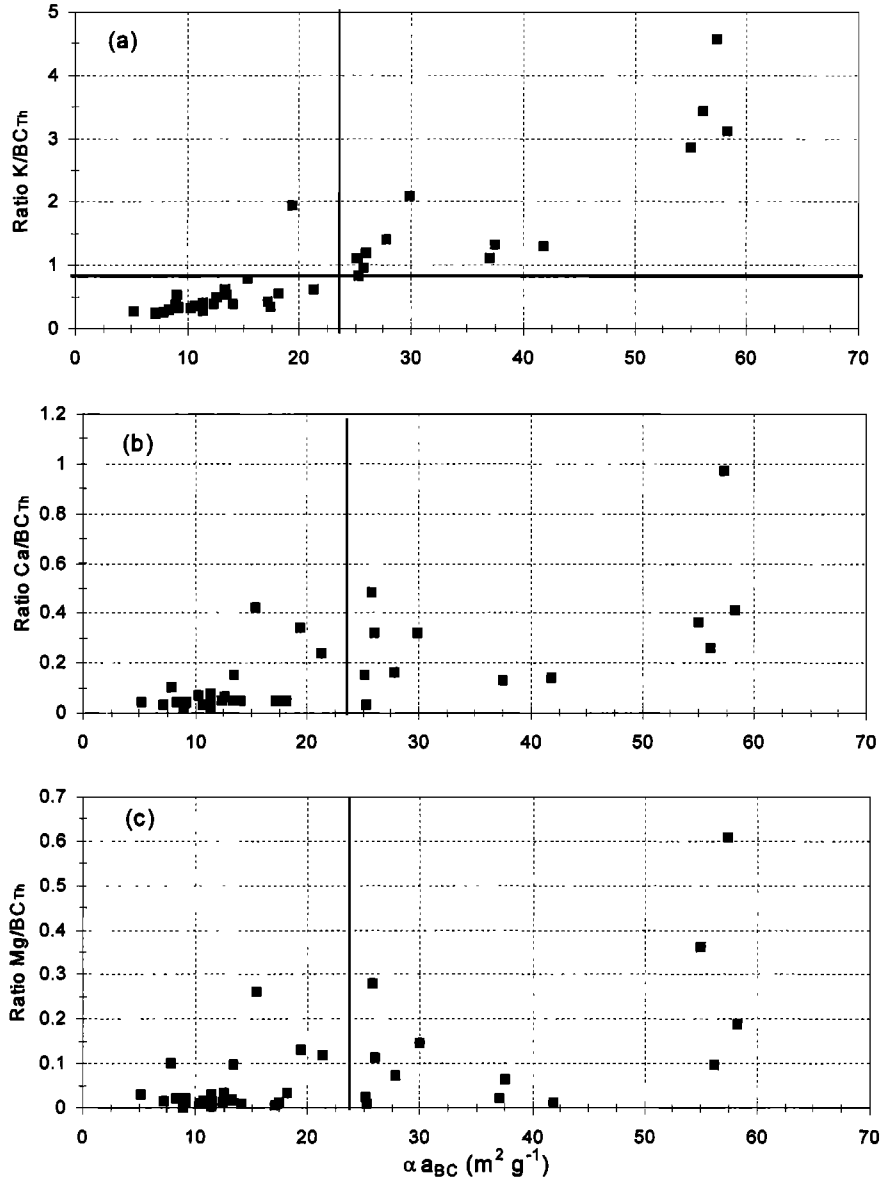

Figure 8. Ratios (a) K/BC_{Th}, (b) Ca/BC_{Th}, and (c) Mg/BC_{Th} versus αa_{BC} for all the analyzed samples. The upper limit $K/BC_{Th} = 0.78$ is pointed in the figure showing the separation for reliable αa_{BC} values.

absorbing particles. The modeled results can account for αa_{BC} values between 5 and 25 $m^2\ g^{-1}$, which explains about 70% of the data set and all αa_{BC} values for $K/BC_{Th} < 0.78$. Table 1 shows general characteristics of the studied samples. There is no clear correlation between αa_{BC} and location, type of combustion, or type of sample. On the other hand, SEM pictures of the samples also suggest a separation in two groups of particles with distinct micromorphology. The first group, which has low αa_{BC} values, has spherical-like shape and relatively homogeneous particles (Figure 10a). The second group, which has high αa_{BC} values, shows a large concentration of nonspherical particles and compact clusters of small particles (Figure 10b), similar to the one shown in Figure 5.

Figure 11 shows an example of the particle size distribution, and the DMPS "hot" size distribution, which corresponds to the size distribution of the same sample after heating the aerosol to 340°C (which causes most volatile compounds to evaporate; for example, organics, ammonium sulfate, etc.). The comparison between the "hot" and the "cold" size distributions suggested a predominance of internal mixing between volatile and nonvolatile particles. Despite the large difference in the size distributions for the "hot" and "cold" samples, the total number of particles was reduced by only 15% by heating, showing that most of the particles were not completely volatile and suggesting internal mixing. Figure 11 shows good agreement between particle count distribution measured with the DMPS and PCASP, despite the fact that the DMPS measures particle sizes on the basis of the electrical mobility of the particles, and the PCASP measurements are derived from light scattering. Volume size distributions calculated from the measured number size distributions, in combination with mass concentration measurements, were used to estimate particle density. Backscattering measurements from the nephelometer were used to estimate the asymmetry factor (g) as a function

Table 1. Characteristics of SCAR-B Samples Listed in Order of BC Mass Absorption Efficiency

Sample	Location of Sampling	Type of Sample	MCE	BC Mass Absorption Efficiency, $m^2\ g^{-1}$	BC_{Th}/TPM, %
1	Brasília	emission factor		5.2	5.85
2	Cuiabá	regional haze		7.2	12.94
3	Cuiabá	Cu processed (fire top)		7.9	4.32
4	Marabá	smoldering (EF)	0.881	8.3	7.10
5	Porto Velho	background		8.9	5.56
6	Brasília	emission factor	0.949	9.1	5.18
7	Marabá	in cloud		9.2	14.07
8	Cuiabá	regional haze		10.3	5.98
9	Porto Velho	background		10.7	2.25
10	Porto Velho	regional haze		11.4	4.60
11	Cuiabá	regional haze		11.4	4.59
12	Marabá	regional haze		11.4	5.76
13	Brasília	emission factor		12.3	9.73
14	Brasília	emission factor	0.936	12.5	5.78
15	Brasília	emission factor	0.958	13.3	10.74
16	Marabá	emission factor	0.896	13.4	7.00
17	Porto Velho	regional haze		14.1	5.03
18	Porto Velho	emission factor	0.894	15.4	4.19
19	Cuiabá	regional haze		17.1	1.85
20	Marabá	emission factor	0.883	17.4	4.41
21	Marabá	emission factor	0.828	18.1	5.05
22	Marabá	emission factor	0.946	19.3	5.82
23	Marabá	emission factor		21.3	6.51
24	Marabá	in cloud		25.1	7.98
25	Porto Velho	emission factor	0.975	25.2	11.82
26	Cuiabá	smoke column		25.7	3.77
27	Marabá	emission factor	0.920	25.9	5.41
28	Porto Velho	regional haze		27.8	1.87
29	Brasília	emission factor	0.949	29.9	4.00
30	Marabá	emission factor		37.0	2.20
31	Marabá	regional haze		37.5	2.33
32	Cuiabá	regional haze		41.9	0.57
33	Marabá	emission factor	0.966	55.0	1.89
34	Marabá	in cloud		56.2	3.15
35	Marabá	emission factor		57.3	1.93
36	Marabá	emission factor	0.855	58.3	2.23

Sample numbers are the same as in Table 2. Note that MCE corresponds to modified combustion efficiency.

of the particle geometric standard deviation, using the expression proposed by *Marshall et al.* [1995]. The real refractive indices of the nonabsorbing shells were estimated in an iterative process to fit the scattering coefficient (σ_s) measured by the nephelometer at a wavelength of 0.55 μm. The amount of BC was allowed to vary until it fitted the absorption coefficient (σ_a) estimated from the Nuclepore filters. After convergence, σ_s, σ_a, the BC content, g, and αa_{BC} were compared with the measured values.

Table 2 shows comparisons between some of the modeling results and the measurements. The average real refractive index obtained from the model was 1.48 ± 0.08 (varying between 1.37 and 1.59). A real refractive index as small as 1.37 can be explained by possible underestimates of σ_s by the nephelometer, uncertainties in the particle size distribution, or inconsistencies between the modeled particle structure and shape (layered sphere) and the actual particles. However, the single-scattering albedo (ω_0) and the asymmetry factor are relatively well produced by the model. The BC content estimated from the model showed poor agreement with the measured BC_{Th}. Large uncertainties in the BC determination from the model are associated to some extent with large values of αa_{BC} de-

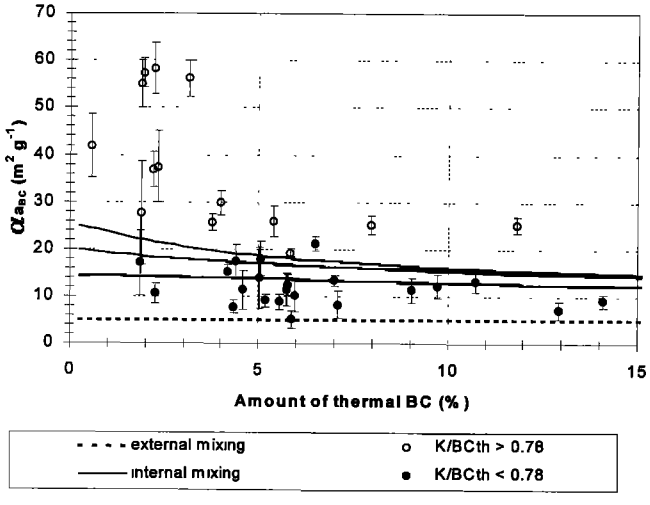

Figure 9. Measured and modeled BC mass absorption efficiencies (αa_{BC}) at $\lambda = 0.55$ μm versus the amount of BC in the sample. Solid curves represent the modeled αa_{BC} for three particle size distributions given in Table 1. The dashed line is the asymptotic limit for αa_{BC} assuming external mixing and for the measured particle size distributions.

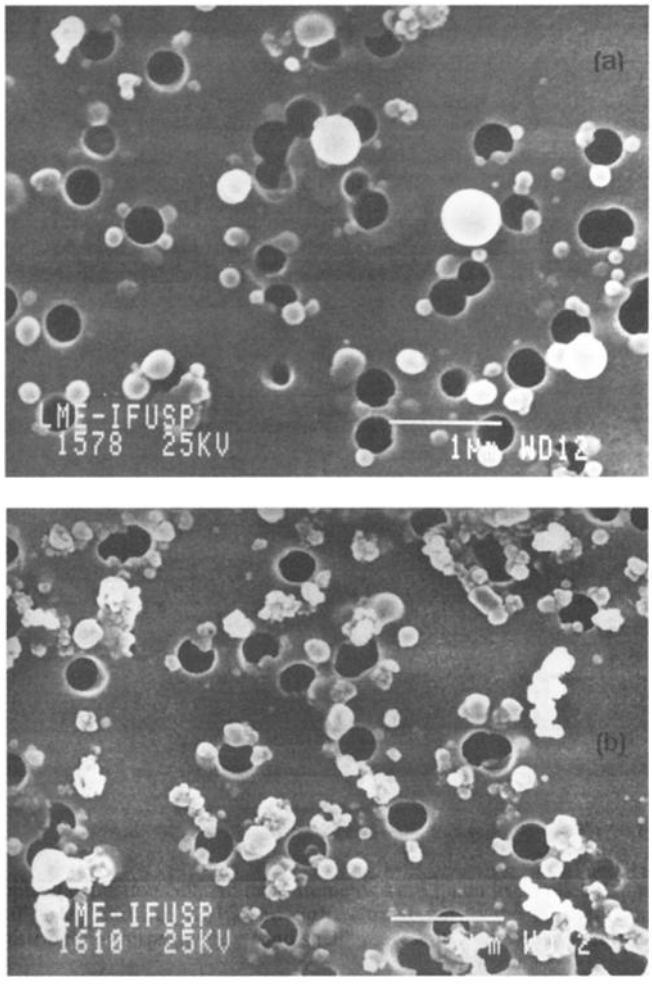

Figure 10. (a) Typical scanning electron microscopy (SEM) photograph of aerosol particles with low αa_{BC} values. Most of the particles have spherical-like shape. (b) Typical SEM photograph of smoke particles with high αa_{BC} values. The photograph shows a large concentration of nonspherical particles and compact clusters of small particles similar to the one shown in Figure 5.

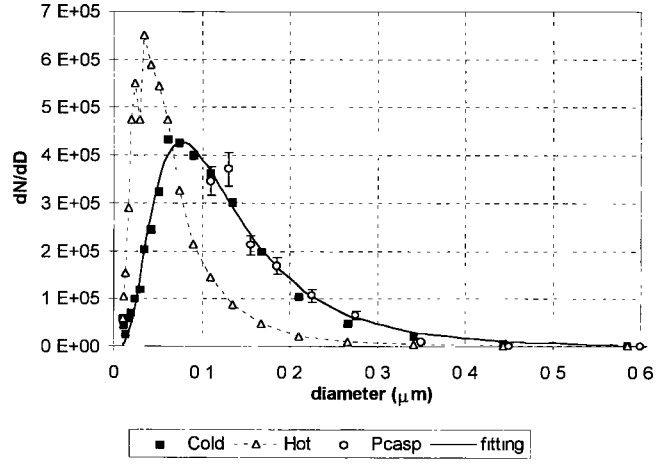

Figure 11. Measured particle size distributions from the DMPS (differential mobility particle sizer) and from the PCASP (passive cavity aerosol spectrometer probe). DMPS cold corresponds to measurements at ambient temperature and hot to measurements at 340°C. The solid curve represents a lognormal fit to the combined DMPS "cold" plus PCASP data. The difference between DMPS results cold and hot suggests predominance of internal mixing.

rived from the combination of the thermal technique and optical absorption measurements (e.g., sample 27). Recall that the model cannot explain values of αa_{BC} larger than 25 $m^2 g^{-1}$ for the particle size distributions considered. Even for monodisperse particles an optimized particle size would provide a maximum value of αa_{BC} around 30 $m^2 g^{-1}$, as shown in Figure 3.

4. Conclusions

Black carbon mass absorption efficiency (αa_{BC}) depends strongly on particle mixing, size distribution, and morphology of the particles. In agreement with the literature, results show

Table 2. Optical and Physical Properties of Aerosol Particles Measured and Calculated Using Mie Theory in Actual Samples Collected During SCAR-B Aboard the UW C131-A Aircraft

	Sample 4		Sample 27		Sample 10		Sample 7		Sample 20	
Results	Measured	Calculated	Measured	Calculated	Measured	Calculated	Measured	Calculated	Measured	Calculated
Type	smoldering, Marabá		flaming, Marabá		haze, Porto Velho		in cloud, Marabá		smoldering, Marabá	
Dg	0.12		0.087		0.19		0.12		0.11	
σg	1.89		1.87		1.78		1.79		1.89	
DgV	0.27		0.25		0.52		0.25		0.27	
σgV	1.63		1.62		1.78		1.62		1.67	
ρ, g cm^{-3}	1.21		1.00		1.20		1.28		1.04	
Rind shell		1.440		1.525		1.370		1.587		1.460
σs, m^{-1}	6.4E−4	6.4E−4	1.11E−3	1.11E−3	4.72E−4	4.72E−4	4.9E−4	4.9E−4	8.70E−4	8.66E−4
σa, m^{-1}	1.30E−4	1.30E−4	3.79E−4	3.80E−4	6.75E−5	7.05E−5	1.54E−4	1.54E−4	1.84E−4	1.84E−4
ω_0	0.83	0.83	0.74	0.74	0.87	0.87	0.76	0.76	0.83	0.83
$\%BC_{Th}$	7.1	4.1	5.41	9.6	4.60	4.3	14.07	7.8	4.41	5.3
g	0.533	0.550	0.485	0.490	0.617	0.689	0.52	0.50	0.534	0.55
αa_{BC}, $m^2 g^{-1}$	8.3	15.3	25.9	15.2	11.4	12.5	9.2	16.6	17.4	15.3

The Mie calculations were performed for layered-sphere particles using the code developed by Ackerman and Toon, further improved and made available by W. Wiscombe, NASA GSFC. Size distributions were measured by the PCASP and DMPS instruments, σs and g was obtained by a onboard nephelometer (λ = 0.55 μm), and σa was obtained by a reflectance technique applied to Nuclepore filters intercalibrated with an optical extinction cell. All measurements were taken in parallel. Sample numbers are the same as presented in Table 1. Read 6.4E−4 as 6.4 × 10^{-4}. Dg and σg, DgV, and σgV, correspond to the geometric mean diameter and standard deviation of the number and volume size distribution, respectively. "Rind shell" represents estimates for refractive index of the nonabsorbing shell.

that the mass of BC was underestimated for samples with high-K content producing unrealistic high values for BC mass absorption efficiencies. An empirical upper limit $K/BC_{Th} = 0.78$ has been defined in this paper to select reliable results for mass absorption efficiencies. Below this value the measured mass of BC_{Th} provided good results for αa_{BC}. Similar behaviors were found for concentrations of Ca and Mg.

The BC mass absorption efficiency (αa_{BC}) for particles from biomass burning in Brazil ranged from 5.2 to 19.3 $m^2 g^{-1}$ with an average value of 12.1 $\pm$ 4.0 $m^2 g^{-1}$. In addition to the layered sphere model for internal mixtures, a packed cluster model was proposed for biomass burning particles from regional haze. For a particular case with BC/TPM = 0.64, the packed cluster structure presented αa_{BC} values up to 35% higher than results obtained for the layered sphere model for particles with radius above 0.1 μm. Modeled results using cluster and layered sphere models plus Mie theory accounted for αa_{BC} values between 5 and 25 $m^2 g^{-1}$ depending on the size distribution and BC fraction. The modeled results provided good estimates for the optical properties of the biomass burning aerosol collected in Brazil. The large range of αa_{BC} measured for biomass burning particles must be taken into account when using optical measurements to determine the mass of BC. An accurate determination of the mass of BC through optical methods depends on knowing the value of αa_{BC} very well for each particular type of particles. Estimates of αa_{BC} are also important to connect BC emissions with light absorption by particles in the atmosphere.

There was no clear correlation between αa_{BC} and location, type of combustion, or type of sample. Samples with low αa_{BC} values contained mostly homogeneous particles with spherical-like shape. Samples containing asymmetrical particles and cluster-like structures showed higher αa_{BC} values. This characteristic was attributed either to the particular internal mixing contributing to enhance the light absorption properties or to earlier volatilization of BC particles during the thermal measurements also enhanced by the particular internal mixing.

Acknowledgments. J. V. Martins thanks the Brazilian agencies FAPESP (project 93/5017-3 and 96/2672-9) and CAPES (project 437/95) for financial support. The University of Washington's participation in SCAR-B was supported by the following grants: NASA NAGW-3750 and NAG 11709; NSF ATM-9400760, ATM-9412082, and ATM-9408941; NOAA NA37RJ0198AM09; and EPA CR822077. We thank Alcides C. Ribeiro, Ana L. Loureiro, and Tarsis Germano for assistance during sampling and analysis. We are very grateful to Hélène Cachier for her careful review and important discussions improving the contents of the paper.

References

Ackerman, P. T., and O. B. Toon, Absorption of visible radiation in the atmosphere containing mixtures of absorbing and nonabsorbing particles, *Appl. Opt.*, *20*, 3661–3667, 1981.

Bohren, C. F., and D. R. Huffman, *Absorption and Scattering of Light by Small Particles*, pp. 213–219, Wiley Intersci., New York, 1983.

Cachier, H., M. P. Brémond, and P. Buat-Ménard, Determination of atmospheric soot carbon with a simple thermal method, *Tellus, Ser. B*, *41*, 379–390, 1989.

Campbell, D., and T. Cahill, Response to "Comment on 'Measurement of aerosol absorption coefficient from Teflon filters using the integrating plate and integrating sphere techniques' by D. Campbell, S. Copeland, and T. Cahill" by A. Clarke, J. Ogren, and R. Charlson, *Aerosol Sci. Technol.*, *24*, 225–229, 1996.

Campbell, D., S. Copeland, and T. Cahill, Measurements of aerosol coefficient from Teflon filters using integrating plate and integrating sphere techniques, *Aerosol Sci. Technol.*, *22*, 287–292, 1995.

Chylek, P., G. Videen, D. Ngo, R. G. Pinnick, and J. D. Klett, Effect of black carbon on the optical properties and climate forcing of sulfate aerosols, *J. Geophys. Res.*, *100*, 16,325–16,332, 1995.

Clarke, A. D., Integrating sandwich: A new method of measurement of the light absorption coefficient of atmospheric particles, *Appl. Opt.*, *21*, 3011–3021, 1982a.

Clarke, A. D., Effects of filter internal reflection coefficient on light absorption measurements made using the integrating plate method, *Appl. Opt.*, *21*, 3021–3031, 1982b.

Clarke, A. D., K. J. Noone, J. Heintzenberg, S. G. Warren, and D. S. Covert, Aerosol light absorption measurement techniques: Analysis and intercomparisons, *Atmos. Environ.*, *21*, 1455–1465, 1987.

Clarke, A. D., J. Ogren, and R. Charlson, Comment on "Measurement of aerosol absorption coefficient from Teflon filters using the integrating plate and integrating sphere techniques" by D. Campbell, S. Copeland, and T. Cahill, *Aerosol Sci. Technol.*, *24*, 221–224, 1996.

Delumyea, R. G., L. C. Chu, and E. Macias, Determination of elemental carbon component of soot in ambient aerosol samples, *Atmos. Environ.*, *14*, 647–652, 1980.

Draine, B. T., and P. J. Flatau, Discrete dipole approximation for scattering calculations, *J. Opt. Soc Am. A.*, *11*, 1491–1499, 1994.

Hallet, J., J. G. Hudson, and C. F. Rogers, Characterization of combustion aerosols for haze and cloud formation, *Aerosol Sci. Technol.*, *10*, 70–83, 1989.

Hanel, G., Single scattering albedo, asymmetry parameter, apparent refractive index, and apparent soot content of dry atmospheric particles, *Appl. Opt.*, *27*, 2287–2294, 1988.

Hanel, G., and C. Hillenbrand, Calorimetric measurements of optical absorption, *Appl. Opt.*, *28*, 510–516, 1989.

Hanel, G., R. Busen, C. Hillenbrand, and R. Schloss, Light absorption measurements: New techniques, *Appl. Opt.*, *21*, 382–386, 1982.

Hansen, A. D. A., H. Rosen, and T. Novakov, Real time measurement of the aerosol particles, *Appl. Opt.*, *21*, 3060–3062, 1982.

Hobbs, P. V., Summary of types of data collected on the University of Washington's Convair C-131A aircraft in the Smoke, Clouds and Radiation-Brazil (SCAR-B) field study from 17 August–20 September 1995, Cloud and Aerosol Res. Group, Dep of Atmos. Sci., Univ. of Washington, Seattle, March 1996. (Also available on http://cargsun2.atmos.washington.edu/.)

Horvath, H., Atmospheric light absorption—A review, *Atmos. Environ., Ser. A*, *27*(3), 293–317, 1993a.

Horvath, H., Comparison of measurements of aerosol optical absorption by filter collection and a transmissometric method, *Atmos. Environ., Ser. A*, *27*, 319–325, 1993b.

Japar, S. M., W. W. Brachaczek, R. A. Gorse, J. M. Norbeck, and W. R. Pierson, The contribution of elemental carbon into the optical properties of rural atmospheric aerosols, *Atmos. Environ.*, *20*, 1281–1289, 1986.

Lindberg, J. D., and L. S. Laude, Measurement of the absorption coefficient of atmospheric dust, *Appl. Opt.*, *13*, 1923–1927, 1977.

Liousse, C., H. Cachier, and S. G. Jennings, Optical and thermal measurements of black carbon aerosols content in different environments: Variations of the specific attenuation cross section, sigma (σ), *Atmos. Environ., Ser. A*, *27*, 1203–1211, 1993.

Marshall, S. F., D. S. Covert, and R. J. Charlson, Relationship between asymmetry parameter and hemispheric backscatter ratio: Implications for climate forcing by aerosols, *Appl. Opt.*, *34*, 6306–6311, 1995.

Martins, J. V., P. V. Hobbs, R. E. Weiss, and P. Artaxo, Sphericity and morphology of smoke particles from biomass burning in Brazil, *J. Geophys. Res.*, this issue.

Novakov, T., and C. E. Corrigan, Thermal characterization of biomass smoke particles, *Mikrochim. Acta*, *119*, 157–166, 1995.

Patterson, E. M., and B. T. Marshall, Diffuse reflectance and transmission measurements of aerosol absorption, in *Light Absorption by Aerosol Particles*, edited by H. E. Gerger and E. E. Hindman, Spectrum, Hampton, Va., 1982.

Petzold, A., and R. Niessner, Method comparison study on soot-selective techniques, *Mikrochim. Acta*, *117*, 215–237, 1995.

Purcell, E. M., and C. R. Pennypacker, Scattering and absorption of light by nonspherical dielectric grains, *Astrophys. J.*, *186*, 705–714, 1973.

Reid, J. S., and P. V. Hobbs, Physical and optical properties of young smoke from individual biomass fires in Brazil, *J. Geophys. Res.*, this issue.

Reid, J. S., P. V. Hobbs, C. Liousse, J. V. Martins, R. E. Weiss, and

T. F. Eck, Comparisons of techniques for measuring shortwave absorption and the black carbon content of aerosols from biomass burning in Brazil, *J. Geophys. Res.*, this issue (a).

Reid, J. S., P. V. Hobbs, R. J. Ferek, D. R. Blake, J. V. Martins, M. R. Dunlap, and C. Liousse, Physical, chemical, and optical properties of regional hazes dominated by smoke in Brazil, *J. Geophys. Res.*, this issue (b).

Roessler, D. M., and F. R. Faxvog, Optical properties of agglomerated acetylene smoke particles at 0.5145 μm and 10.6 μm wavelengths, *J. Opt. Soc. Am.*, *70*, 230–235, 1980.

Ruoss, K., R. Dlugi, C. Weigl, and G. Hanel, Intercomparison of different Aethalometers with an absorption technique: Laboratory calibrations and field measurements, *Atmos. Environ.*, *27A*(8), 1221–1228, 1993.

Weiss, R. E., and P. V. Hobbs, Optical extinction properties of smoke from the Kuwait oil fires, *J. Geophys. Res.*, *97*, 14,537–14,540, 1992.

P. Artaxo and J. V. Martins, Instituto de Física, Universidade de São Paulo, C.P. 66318, CEP 05315-970, São Paulo, Brazil. (e-mail: vanderlei@if.usp.br)

P. V. Hobbs and J. S. Reid, Department of Atmospheric Sciences, University of Washington, Seattle, WA 98195-1640.

Y. Kaufman, NASA Goddard Space Flight Center, Code 913, Greenbelt, Maryland 20771.

C. Liousse, Centre de Faibles Radioactivites, CNRS-CEA, Av de la Terrasse, 91198 Gif sur Yvette, France.

(Received October 6, 1997; revised July 1, 1998; accepted August 3, 1998.)